Journal of Manufacturing Processes 47 (2019) 284–290

Contents lists available at ScienceDirect

Journal of Manufacturing Processes

journal homepage: www.elsevier.com/locate/manpro

Development of an open-sourced automated ultrasonic-assisted soldering system

J. Shaffer, K. Maassen, C. Wilson, P. Tilton, L. Thompson, H. Choi, J. Bostwick*

Clemson University, Fluor Daniel Building, 29634, Clemson, SC, United States

ARTICLE INFO

Keywords:
Ultrasonic-Assisted soldering
Automated system
Wetting behavior

ABSTRACT

As the electronics, automobile and other industries seek to eliminate the use of flux when joining dissimilar materials, ultrasonic-assisted soldering (UAS) has emerged as a prime candidate to replace conventional soldering to improve wetting at bonded joint surfaces. A challenge for UAS is to effectively scale up techniques for industrial use. This paper presents a modular, open-sourced automated system that was designed to allow for flexible and repeatable experimentation of the UAS process. Key process parameters include solder tip speed, tip distance from the substrate, ultrasonic power supplied to the molten solder, and the extrusion rate of the solder onto the substrate. Each of these parameters are user-controlled in our automated system, which is capable of soldering a general curved path while maintaining leading-edge orientation of the soldering tip. A compatible, low-cost profilometer attachment is retrofitted to our system in order to non-destructively characterize the wetting behavior of the solder-substrate system.

1. Introduction

Ultrasonic-assisted soldering (UAS) is a process for joining difficult-to-solder materials without the use of environmentally-harmful flux, which is traditionally used to enhance wetting of the solder materials [1,2]. Flux residue is also expensive to remove in post-processing operations and contributes to voiding in soldered joints. UAS negates the need for flux through an alternative mechanism [3]. Ultrasonic energy applied to the molten solder pool causes the rapid formation and collapse of cavitation microbubbles, which creates localized areas of extremely high temperature and pressure that remove the surface oxide layer (`scrubbing action') of the metallic substrate and improves solder wettability. This multiphysics process involves solidification (phase change), heat transfer, acoustics, fluid mechanics, and surface science (wetting and adhesion), and is schematically illustrated in Fig. 1a. Several critical process parameters that affect the solder joint quality of UAS are summarized in Fig. 1b [2,4,6–8,10,12].

Due to the complex interactions of the UAS process parameters, it is difficult to reliably perform manual soldering by hand. Along the same lines, it is difficult to optimize the UAS process without the ability to precisely control the process parameters. We address this critical gap in the literature through the design of an automated UAS system with precise control over a large number of process parameters.

Our motivation is to produce a scalable, open-sourced, and modular soldering system design, which allows for maximum flexibility while maintaining precise control of the UAS process parameters. Recent work includes an automated system consisting of a visual monitoring system with XY-motion stage, commercial soldering iron, and solder feed unit [9]. However, this lab-scale system has a limited build space and lacks precise control of the extruded solder volume. In the current market, there are many handheld ultrasonic soldering units available but only one primary manufacturer of automated ultrasonic soldering equipment, Japan Unix Co, Ltd. The total cost of the commercial automated system with comparable features is upwards of 75,000 USD, though it does provide a patented system capable of providing closed-loop feedback in the event of a solder jam in their extrusion system which our system currently lacks. Our automated UAS system is built around a heavily modified fused deposition modeling (FDM) printer base, which increases system flexibility/modularity and allows for vendor-choice of parts. Both features allow for a relatively low-cost system design in comparison to the commercial system. Our total system costs less than 20,000 USD. In addition to affordability, our system incorporates novel features such as a solder wire extruder system and an integrated profilometer for characterization of solder lines. Lastly, due to its modular design, the automated UAS system is easy to maintain and operate.

Currently, UAS is widely used in the automobile and electronics industries, but is limited to ultrasonic baths, reflow soldering, or spot

* Corresponding author.
E-mail address: jbostwi@clemson.edu (J. Bostwick).

https://doi.org/10.1016/j.jmapro.2019.09.007
Received 11 May 2019; Received in revised form 6 August 2019; Accepted 5 September 2019
1526-6125/

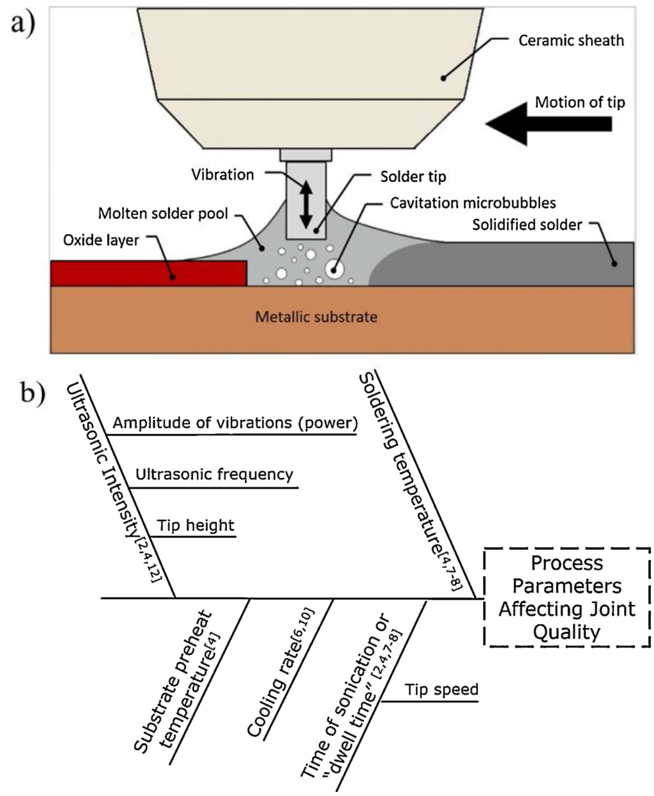

Fig. 1. a) Schematic of the UAS process with metallic substrate and b) its associated process parameters that affect the resulting solder joint quality [2,4,6–8,10,12].

soldering [3,10]. For such applications, hand soldering is sufficient and there is not a critical need to automate. However, as the packaging density of electronic components continues to increase with improved microfabrication technology, there is a critical need for precision soldering equipment that can be industrially scaled. A common practice in modern mass production is to use soldering mask to deposit layers of solder on the substrates. Unfortunately, this technique reduces flexibility in the manufacturing and assembly process as design changes require additional costs and lead time for new masks [9,11]. An automated system that effectively deposits solder without the use of masks would greatly improve industrial efficiency and reliability. Furthermore, our solder extruder system can greatly reduce material waste with associated large cost savings of expensive low-temperature solders.

The mechanism for improved wettability and accelerated bonding in UAS is well-established in the literature for metallic substrates [4,12,13]. However, there are comparably few studies on the implementation of UAS with glass substrates [14]. Here we are interested in using our UAS system to study the wetting behavior on silica glass substrates. Most traditional solder alloys tend to exhibit hydrophobic behavior and create solder beads on glass substrates, which we will hereafter refer to as solder lines. For a given cross section of the solder line, the width and height describe the spreading in the horizontal and vertical directions, respectively, while the contact angle α between the substrate and meniscus describes the relative balance of interfacial energies [15]. For reference, our typical solder lines have a width of 3 mm and height of 0.15 mm. To resolve the cross-sectional geometry, we use serial polishing (optical micrographs) and also develop a simple, handcrafted profilometer that integrates directly into our automated UAS system. We validate our profilometer measurements against the optical micrographs. The advantage of our profilometer is that we can non-destructively characterize the solder line geometry (wetting behavior) in a timely manner.

We begin this paper by providing a broad overview of our automated UAS system and its component subsystems, where we define how our system is able to control the process parameters. The materials and protocols used to evaluate the automated UAS system and quantifying the solder quality are then described. We then present and discuss our validation results for leading-edge soldering, solder extrusion rate, repeatability, and geometric characterization of the solder line topography. Finally, some concluding remarks are offered regarding areas of system improvement.

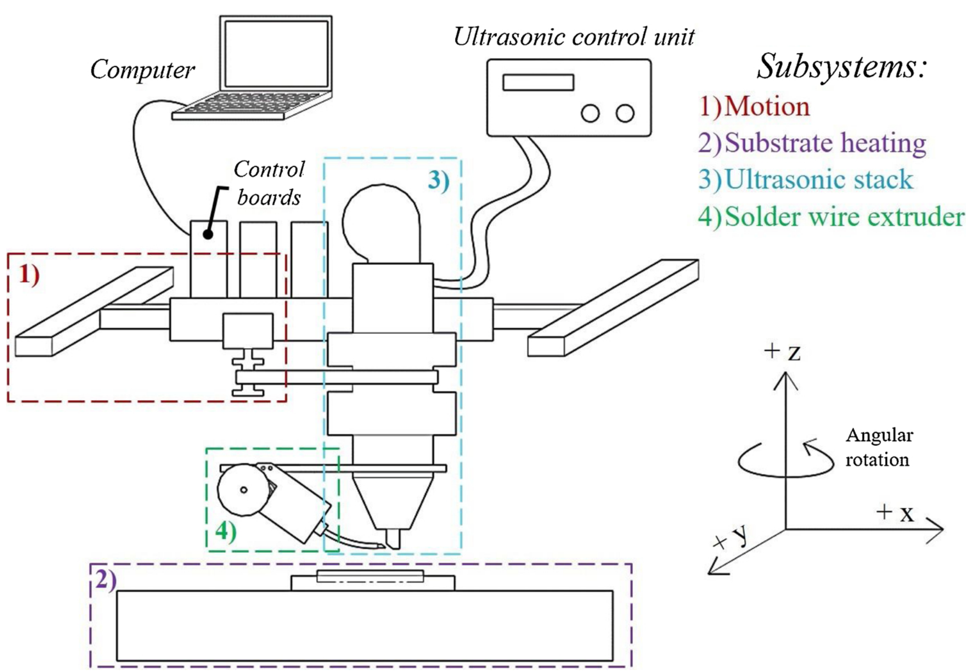

Fig. 2. Schematic of the full assembly decomposed into associated subsystems.

2. Overview of automated UAS system

The automated UAS system was built by heavily modifying an existing, commercial-scale benchtop model FDM machine base with a heated base (Hydra 340, Hyrel 3D). A system-level schematic is shown in Fig. 2, which defines the four primary subsystems: motion, substrate heating, ultrasonic stack, and solder wire extruder. The respective subsystems independently control one or more aspects of the UAS process defined in Fig. 1b which we list below and describe later:

1 Motion

- Precise positioning in the X-, Y-, and Z-axis via a gantry and lift system
- Speed of the soldering tip as it moves across a general path
- Distance between the soldering tip and substrate
- Rotation of ultrasonic stack about the Z-axis to maintain leading edge

2 Substrate heating

- Pre-heating temperature

3 Ultrasonic stack

- Amplitude and frequency of the ultrasonic tip vibrations
- Temperature of the piezo-electric transducer
- Temperature of the soldering tip

4 Solder wire extruder

- Extruded solder volume onto substrate

Note the i) ultrasonic energy intensity and ii) ultrasonication time are factors that cannot be directly controlled as process parameters by the automated UAS system. However, they are derivatives of several controllable parameters, such as solder tip speed, tip distance to substrate, amplitude/frequency of ultrasonic vibrations, and the geometry of the soldering tip.

Our automated system incorporates three particularly novel features; 1) rotational control of the ultrasonic stack for leading-edge soldering, 2) volume control of solder, and 3) a simple handcrafted profilometer to characterize the solder line geometry, which we discuss in a later section.

2.1. Motion

A commercial-scale benchtop model FDM machine base provides precise motion control with closed-loop feedback. The custom UAS assembly is attached to an overhead gantry system with positional resolution and accuracy in the X- and Y- directions of 6 μm and 30 μm, respectively. The overhead gantry system allows the ultrasonic soldering tip to move over the substrate at speeds up to 3000 mm/min within a large working area of 300 mm by 400 mm by 250 mm, which makes the system compatible with a wide range of material sizes and sample geometries. The motion stage in the FDM machine base provides precise control in the Z- direction with positional resolution and accuracy of 1 μm and 5 μm, respectively. This allows one to set the solder tip height above the substrate. A unique design feature of our system is that the proprietary solder tip geometry is not multidirectional in nature; thus, the orientation of the solder tip must be maintained along the path. A belt and pulley system driven by a stepper motor is implemented to provide rotational control of the ultrasonic stack about the Z-axis in order to maintain the leading edge along a general curved path.

2.2. Substrate heating

A custom standalone heated-base was designed and fabricated out of aluminum to i) constrain the motion of the glass substrate in the lateral directions and ii) replace the commercial heated base in order to reduce the substrate preheating time to the desired temperature (up to 200 °C). Internal high-density heater cartridges (MCH2-40W-002, Comstat, Inc.) provide heating to the desired temperature, which is actively monitored by a platinum RTD (100Ω, Omega Engineering) to avoid overheating of the substrate.

2.3. Ultrasonic stack

Mounted directly to the overhead gantry system (where the FDM nozzle would traditionally be) is a proprietary ultrasonic soldering stack that provides undamped longitudinal vibrations to the solder tip at frequency $f = 60 \pm 5$ kHz. The amplitude of vibration ranges from 0 to 5 μm and is controlled by the power provided by a phase-locked amplifier within the commercial ultrasonic soldering control unit (Sunbonder USM-IV, Kuroda Techno Co., Ltd.). The operating temperature of the solder tip is 190 °C, which is monitored with a platinum RTD (100Ω, Omega Engineering) to avoid system overheating. We observed that an elevated temperature of the piezoelectric transducer produced thermal drift of the ultrasonic frequency and power. A cooling subsystem was then implemented within the ultrasonic stack to reduce the piezoelectric temperature rise. As described above, the proprietary solder tip geometry is optimized for ultrasonic energy concentration and has an orientation that is maintained throughout the motion by a belt and pulley system that provides Z-axis rotational control of the complete solder stack assembly.

2.4. Solder wire extruder

Our UAS system introduces a novel, low-cost method to control the extruded volume of solder onto the substrate while maintaining a leading edge. A solder wire extruder subsystem has been mounted directly to the rotating ultrasonic stack assembly and has been designed to guide the flow of solder directly into the leading edge of the soldering tip. Note that the extruder rotates with the stack. The extruder subsystem interfaces directly with the 3D-printing software (Repetrel, Hyrel 3D), so the feed rate can be controlled precisely. Extensive testing was performed to establish and calibrate the volumetric feed rate in order to predictably extrude a known solder volume onto a substrate. We discuss these results in detail later. The primary component of this subsystem is a heavily modified FDM Bowden extruder with a 16-gauge stainless steel hypodermic needle to guide the solder into the tip. Our testing has shown that the solder wire extruder is compatible with a wide range of solder wire diameters to allow for a flexible selection of solder alloys, provided their liquidus temperatures are below 200 °C.

3. Material and methods

Our automated UAS system was designed to control a large number of process parameters. For the purposes of this paper, we are interested in ultrasonic soldering onto glass substrates and quantifying the geometry of the solder line to better understand how wetting is affected by the ultrasonic field. By evaluating the geometry, we are able to validate the control of the process parameters in our system. In this section, we describe a cleaning/preparation procedure for the glass substrates and define the type of solder used during testing. We characterize the solder line geometry through both serial polishing and a simple handcrafted profilometer that interfaces directly with our UAS system.

3.1. Preparation of samples

Since the surface condition of the substrates strongly influences the

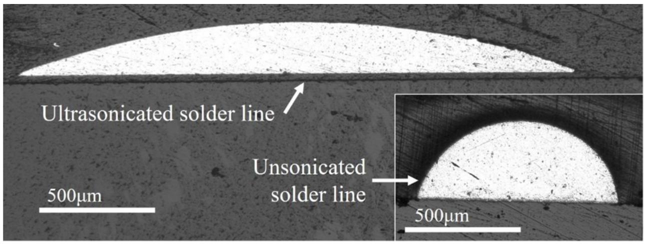

Fig. 3. Cross-sectional images contrasting sonicated and unsonicated solder lines.

solder joint strength, the silica glass used in this study is cleaned in sequential steps using acetone, isopropyl alcohol, and deionized water in an ultrasonic bath for three minutes to remove organic and inorganic contamination from the surface [4,5,10,16,17]. The solder alloy selected for the validation tests is an active Bi-Sn alloy (S-Bond 140 M1, S-Bond Technologies) with a wire diameter of 13.97 mm and a joining temperature between 150 °C and 160 °C.

3.2. Characterization of samples

UAS enhances the solder wettability and improves the bond strength through increasing the solder/substrate contact area [18]. This is clearly seen in Fig. 3 which contrasts the cross-sectional geometry of a sonicated and unsonicated solder line. The geometry of the cross section defines the wetting behavior through the width, height, cross-sectional area, and contact angle. We utilize two techniques to characterize the geometry and equivalently the wetting properties; serial polishing and profilometry.

Serial polishing is a commonly used technique to quantify geometric features with high-resolution. Samples are prepared using room-temperature curing resin to avoid changing microstructural properties and preserve the shape of the solder line. The cross-sectional sample was then ground using 120, 240, 400, 800-grit silicon carbide abrasive papers, polished using 9 µm, 3 µm, and 1 µm diamond suspensions and lastly polished with a 50 nm alumina suspension. Optical micrographs are then taken with a high-resolution microscope camera (ProgRes Gryphax Arktur, Jenoptik), as shown in Fig. 3, which are analyzed using Gryphax (Jenoptik) and ImageJ (National Institutes of Health) software to measure the cross-sectional geometry. The process is repeated to generate additional cross sections along the length of the solder line. As a result, the serial polishing technique is both time-intensive [often taking hours to gain a few cross-sectional images] and a destructive measurement technique. The advantage is a high-resolution micrograph (Fig. 3).

A simple handcrafted, low-cost profilometer was designed and implemented into the automated UAS system to quickly and non-destructively measure the topological profile of the solder line. The profilometer is constructed from a digital test indicator (P900-S129, Accusize Industrial) with a resolution of 1 µm that is connected to an Arduino board (Arduino Nano, Arduino), which enables communication from the dial indicator to the computer controlling the UAS system. The dial indicator measures the displacement of the stylus with an accuracy of ± 0.5 µm. Fig. 4a, and b shows the profilometer and a schematic for the measurement process.

A cross-sectional scan generates an array of position (x_n) and height (h_n) measurements (x_n, h_n) that when concatenated define the cross-sectional shape. A three-dimensional profile can be obtained by compiling cross-sectional scans along the length of the solder line. Fig. 4c illustrates a 3D rendering of an atypical solder line. Post-processing allows one to compute height, width, and cross-sectional area (equivalently, volume). For reference, a typical solder line has a length of approximately 70 mm and a width (W) of 2.3 mm.

The precision of a cross-sectional scan is user-defined by the desired resolution in the X (length) and Y (width) directions. Higher resolution requires more data points and results in longer scan times. Preliminary studies suggest a resolution of 2 mm along the length and 0.1–0.2 mm along the width provide accurate topography of a solder line while maintaining reasonable scan times. As the profilometer is directly integrated into the automated system, it has the potential to be used to monitor solder quality (quality control) and act as an early detection system for wetting failure.

4. Results and discussion

Our automated UAS system has the capability to control a large number of process parameters over a wide range of values. Some of these parameters, such as substrate temperature, solder tip temperature, and ultrasonic power/frequency, are actively monitored by our system with precise control and need not be discussed further. In this section, we discuss the ability of our system to perform leading-edge soldering, control solder volume extrusion, and solder line repeatability.

4.1. Leading-edge soldering and motion control

The ability to produce a uniform solder line that adheres to the glass substrate is dependent upon a number of process parameters, most importantly tip speed, solder extrusion rate, and tip height. A number of straight solder line trials were conducted using various values of these process parameters (fixed ultrasonic power) to determine the maximum effective solder tip speed to be 2250 mm/min, or 90% of the maximum speed of the machine. It was also found that the maximum working distance between the solder tip and the substrate should be less than 0.6 mm (approximately the radius of the solder wire). We expect this value to be influenced by the intensity of the ultrasonic field and size of the solder wire, though further studies would need to be performed to confirm. Operating our system outside these parameter values leads to a solder line that does not adhere to the substrate.

As mentioned previously, our solder tip has an orientation that must be maintained along the solder path. We accomplish this rotational-axis control via a stepper motor mounted to the gantry system and interfaced with the system software. This provides 360° of rotation. The full motion (translational and rotational) for the UAS system is controlled by G-code script. Fig. 5 illustrates our system functionality by soldering 'CLEMSON', which requires the soldering tip i) to rotate, ii) move in multiple directions, and iii) stop and start solder extrusion, in order to maintain the leading edge. The orange text overlaying the silver-colored solder represents the expected G-code path. We note the high quality solder lines and agreement with the expected path, with the exception of the slight shift of the S, O, and N, which we attribute to the glass slide shifting (~0.5 mm) in the substrate holder. In particular, the `S' and `O' clearly demonstrate the ability of our system to perform leading edge soldering.

4.2. Solder extruder

One particularly noteworthy aspect of our system is the ability to predictably deposit a fixed amount of solder onto the substrate. This is accomplished via an extruder, as discussed above, that is operated using the system software. Commercial 3D printing software uses quantities like pulses/microliter, nozzle diameter, flow multiplier, etc. to control material feed rates by controlling the number and frequency of pulses of the stepper motor which drives our solder wire extruder. Unfortunately, many of the programming details of the commercial 3D printing software were not available to us due to proprietary reasons and so effectively functioned as a “black box” that drove the stepper motor, so we opted to empirically establish a relationship between these software input values and the actual length of solder that was output in a given amount of time. To do this, we varied the software input values and

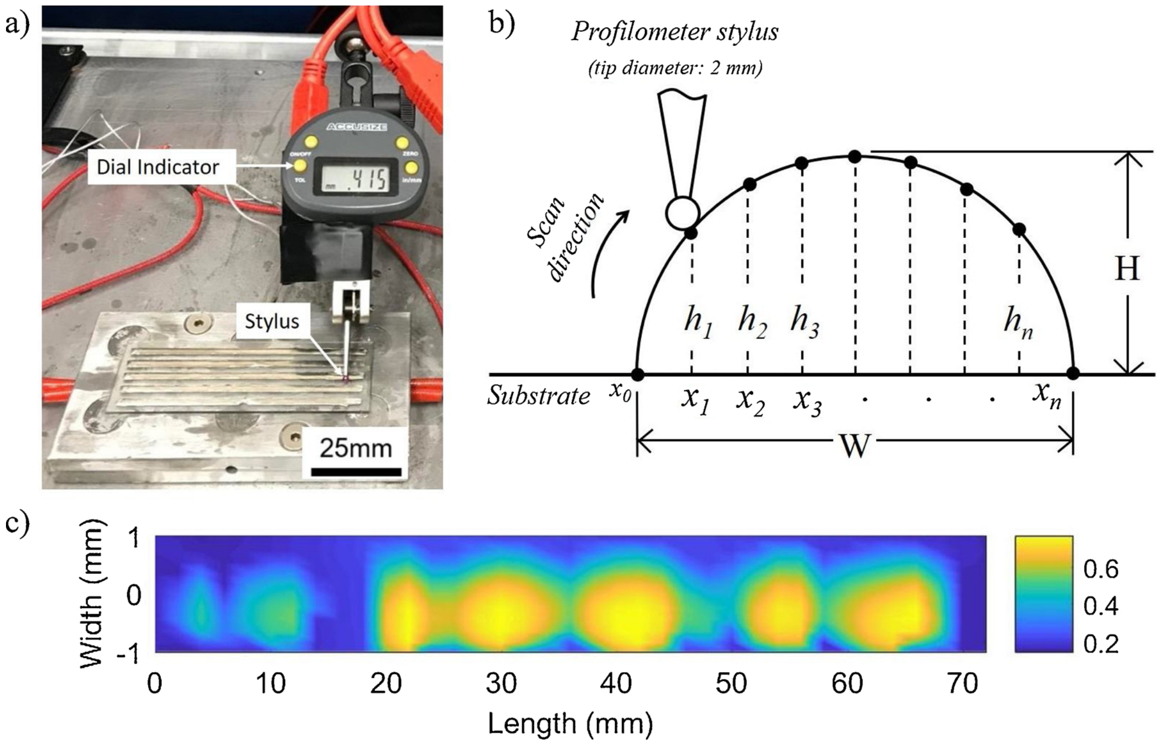

Fig. 4. Simple handcrafted low-cost profilometer is a) directly integrated into the automated system in order to b) measure the cross-sectional geometry along the length of the solder line, which can then be compiled into a c) surface profile.

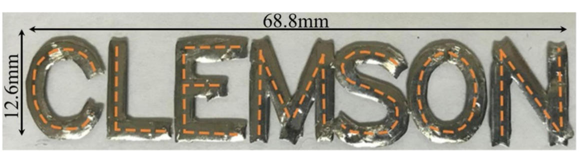

Fig. 5. Demonstration of leading-edge soldering ('CLEMSON') where the orange text represents the centerline of the tip path from the G-code script.

Table 1
Comparison of predicted and actual length of extruded solder under various extrusion settings.

Predicted length [mm]	Actual length [mm]	Percent error [%]
6.36	6.04	5.03
6.36	6.81	7.07
6.36	6.81	7.07
8.48	8.00	5.66
10.6	10.6	0.00
12.7	12.5	1.57
12.7	12.8	0.79
25.4	25.0	1.57
25.4	25.1	1.18

then measured the output length of solder wire in a specified period of time. From this method, we were able to establish a calibration curve to accurately predict what solder feed rate would result from a given combination of software input settings. Several tests were performed to validate our calibration curve; Table 1 shows the length (and equivalently volume) of extruded solder can be predicted within 7% of the actual value.

4.3. Profilometer

The profilometer was validated for accuracy by scanning a 3D printed test surface with known topography. The results of the scan found indicated a 6.5% maximum error in the height and 29% maximum error in the width when considering all topographical shapes. However, for features with widths larger than 1.5 mm, the maximum error was reduced to 16.3%. This was considered an acceptable level of error, considering that nearly all solder line trials have widths larger than 1.5 mm. To resolve finer features, a smaller stylus tip could be used.

4.4. Solder line repeatability

To demonstrate the repeatability of the UAS process, five solder lines were produced using identical system parameters; 4.5 W of ultrasonic power, tip height of 0.2 mm and tip speed of 180 mm/min, all of which are intermediate values of the process parameters (and below the maximum threshold discussed above). These solder lines are shown in Fig. 6. Each solder line was scanned at 26 locations along its length using the profilometer and its profile was rendered. The stability of the process can be evaluated based on the calculated height, width, and cross-sectional area of the 26 cross-sectional scans both within the solder line and across the 5 identical solder lines. Table 2 provides the statistical results for the 5 solder lines, which are quantified using the maximum height (H), width (W) and cross-sectional area with 95% confidence intervals. The statistical variation both within a given solder line and across the 5 solder lines is relatively low, which demonstrates that the UAS system is capable of producing consistent results.

Fig. 6. Solder lines (5x) with identical process parameters on glass substrate demonstrate system repeatability.

Table 2
Comparison of maximum height, width, and cross-sectional area of the five solder lines with identical soldering parameters (cf. Fig. 6) with 95% confidence intervals.

	Maximum height (H) [mm]	Width (W) [mm]	Cross-sectional Area [mm^2]
Line 1	0.184 ± 0.022	3.050 ± 0.293	0.3568 ± 0.0744
Line 2	0.178 ± 0.013	2.708 ± 0.152	0.2748 ± 0.0435
Line 3	0.158 ± 0.014	2.708 ± 0.256	0.2857 ± 0.0646
Line 4	0.156 ± 0.013	2.746 ± 0.233	0.2708 ± 0.0545
Line 5	0.166 ± 0.012	2.815 ± 0.233	0.3092 ± 0.0569
All Lines	0.168 ± 0.018	2.805 ± 0.239	0.2995 ± 0.0602

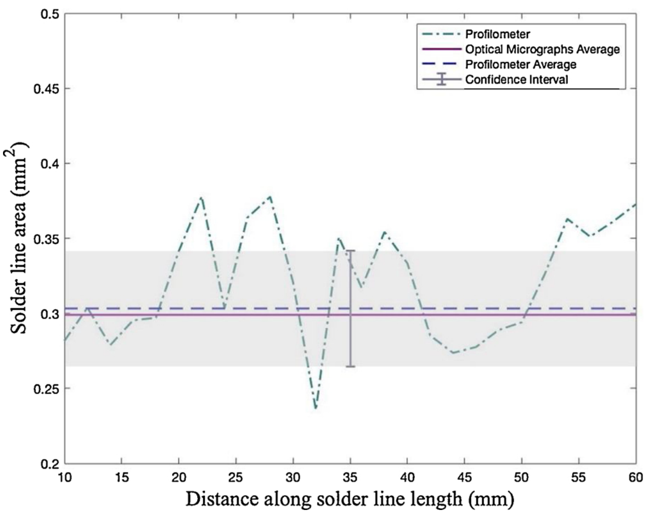

Fig. 7. Cross sectional area along the length of the solder line measured by the profilometer compared with optical micrograph.

4.5. Cross-sectional area validation

Mass conservation dictates the cross-sectional area A of the solder line should remain constant along its length for a fixed solder tip speed v (mm/min) and extrusion rate V (mm^3/min); $A = V/v$ (mm^2). We use the profilometer data to compute the cross-sectional area A using trapezoidal integration. Fig. 7 shows how A varies along the length of a typical solder line, which is fairly uniform. The value from the optical micrograph is superimposed on the graph to validate the use of the profilometer, as well as the area calculation. Note the computed area is equal to the micrograph value at the location along the length where the micrograph was taken.

4.6. Surface roughness

For most trials, the maximum height of the solder line was largely stable along its length, but some variations attributed to defects due to the process, such as accumulation of molten solder on the tip. Such height variations generate a surface roughness which is readily measured using the height data from the profilometer. For example, Fig. 8 plots the height profile of a typical solder line as it depends upon its length. The surface roughness is defined as $ra = \sqrt{\frac{1}{N}\sum_{i=1}^{N} h_i^2}$ or in integral form as $ra = \sqrt{\frac{1}{L}\int_0^L h^2(x)dx}$. For the sample shown in Fig. 8, we use $N = 26$ discrete height measurements along the length to yield a surface roughness of 0.1691 mm. Preliminary experimentation shows the surface roughness increases with the solder tip speed, with all other process parameters held constant (cf. Fig. 9). In contrast, the solder width (wettability) decreases with increasing solder tip speed, as shown in Fig. 10. This suggests it is desirable to keep the tip speed low in order to reduce surface roughness and improved wettability. Future work will

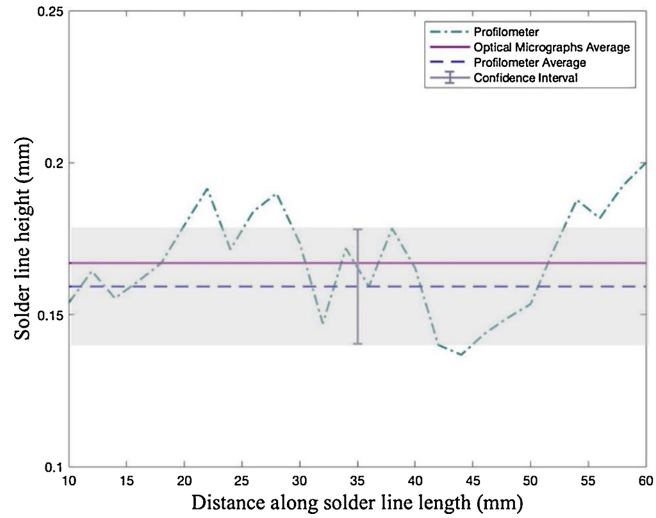

Fig. 8. Height profile along the length of the solder line measured by the profilometer is compared with the optical micrograph and can be used to compute surface roughness.

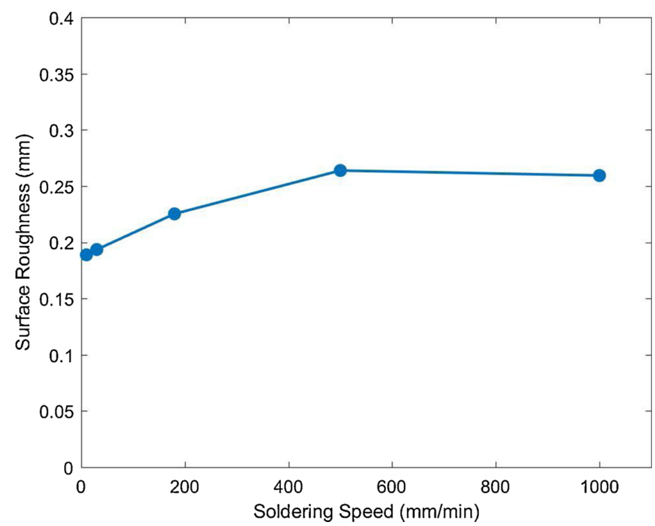

Fig. 9. Preliminary testing shows a correlation between solder tip speed and surface roughness, with all other processing parameters held constant.

focus more heavily on the interaction of the controllable process parameters with the geometries of the solder lines (wettability, surface roughness) to better understand the ultrasonic-assisted soldering process.

5. Conclusion

In this paper, a design for a commercial-scale machine capable of automating the ultrasonic soldering process with a high level of control of a large number of process parameters was presented. The automated system was determined to be stable and provide consistent and repeatable ultrasonic-assisted soldering over a large range of process parameters. The proposed system equipment costs substantially less than the commercial alternative while allowing users to open-source their parts from a variety of vendors and provide easy maintenance and potential scalability with its modular subsystem design.

The most notable achievements of the system presented herein are:

1. The ability to perform leading-edge soldering
2. Control the volume of solder deposited on the substrate
3. The design of a handcrafted, low-cost profilometer that integrates

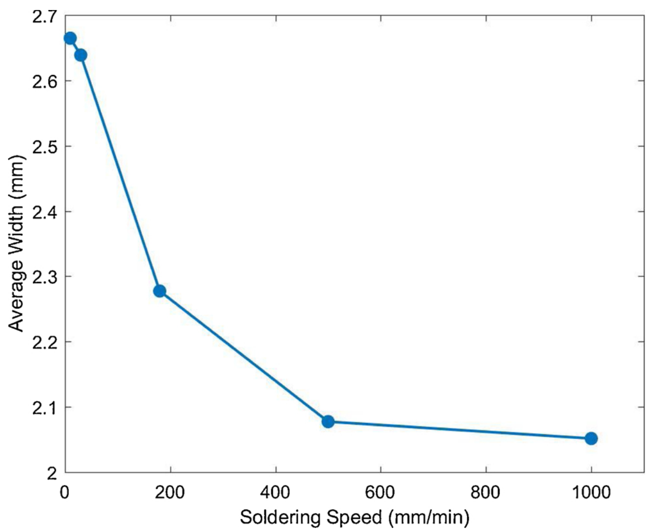

Fig. 10. Preliminary testing shows a correlation between solder tip speed and solder width, with all other processing parameters held constant.

directly into the UAS system to non-destructively characterize the topological profiles of the solder lines with a favorable level of accuracy.

Future work to improve the system includes incorporating i) closed-loop feedback to allow the system to register an extrusion failure (e.g. extruder jams or the solder wire runs out) and ii) an inert gas-flow subsystem to provide a localized protective atmosphere over the solder area to deter oxidation of some solders. With the high level of control and flexibility that this system offers over the UAS process parameters, the system provides a strong foundation for future experimentation and system development for a range of solder-substrate systems.

Acknowledgements

We would like to acknowledge the support of Harris Corporation and the Clemson University Department of Mechanical Engineering (ME) in this research effort. We would also like to acknowledge the work of Clemson ME senior capstone design teams and particularly, Cameron Blevins and Cole Crawford.

References

[1] Lanin VL. Ultrasonic soldering in electronics. Ultrason Sonochem 2001;8:379–85. https://doi.org/10.1016/S1350-4177(01)00065-7.
[2] Tan AT, Tan AW, Yusof F. Effect of ultrasonic vibration time on the Cu/Sn-Ag-Cu/Cu joint soldered by low-power-high-frequency ultrasonic-assisted reflow soldering. Ultrason - Sonochemistry 2017;34:616–25. https://doi.org/10.1016/j.ultsonch.2016.06.039.
[3] Lanin VL. Ultrasonic soldering in electronics: New opportunities. In: Willard TG, editor. Solid State electrochem Nova Science Publishers, Inc.; 2010. p. 201–11. https://doi.org/10.1227/01.NEU.0000313112.49285.47.
[4] Faridi HR. Flux-free ultrasonic soldering of aluminum and stainless steel. Sch Arch 2000.
[5] Dusek K, Placek M, Cepek M, Molhanec M. Beshajova pelikanova I. Ultrasonic soldering, mechanical properties of solder joints. Proc. 40th Int. Spring Semin. Electron. Technol. 2017. https://doi.org/10.1109/ISSE.2017.8000925.
[6] Osório WR, Peixoto LC, Garcia LR, Mangelinck-Noël N, Garcia A. Microstructure and mechanical properties of Sn-Bi, Sn-Ag and Sn-Zn lead-free solder alloys. J Alloys Compd 2013;572:97–106. https://doi.org/10.1016/j.jallcom.2013.03.234.
[7] Cannon M, Klenke B, Zarrow P. Lead-free soldering by hand. Assembly 2007;50:50–5.
[8] Goosey M. Soldering considerations for lead-free printed circuit board assembly - an envirowise guide. Circuit World 2005;31:40–4. https://doi.org/10.1108/03056120510585063.
[9] Venkatesan V, Cappelleri DJ. Development of an automated flexible micro-soldering station. Proc. ASME 2017. Int. Des. Eng. Tech. Conf. Comput. Inf. Eng. Conf. 2017. https://doi.org/10.1115/DETC2017-68107.
[10] Hashemabad SG, Gu Z, Ando T. Flux-less direct soldering of aluminum by ultrasonic surface activation. J Mater Process Tech 2016;233:135–41. https://doi.org/10.1016/j.jmatprotec.2016.02.015.
[11] Plummer JR, Lunt BM. A flexible automated solder-paste dispensing system. Proc. 2004 ASEE Annu. Conf. Expo. 2004.
[12] Kang SK, Choi WK, Yim MJ, Shih DY. Studies of the mechanical and electrical properties of lead-free solder joints. J Mater Eng 2002;31:1292–303.
[13] Li Z, Xu Z, Ma L, Wang S, Liu X, Yan J. Cavitation at filler metal/substrate interface during ultrasonic-assisted soldering. Part II: cavitation erosion effect. Ultrason Sonochem 2019;50:278–88.
[14] Xu Z, Li Z, Qi Y, Yan J. Soldering porous ceramics through ultrasonic-induced capillary action and cavitation. Ceram Int 2019.
[15] de Gennes P. Wetting: statics and dynamics. Rev Mod Phys 1985;57:827–63. https://doi.org/10.1103/RevModPhys.57.827.
[16] Palaniappan SCK. A study on process, strength and microstructure analysis of low temperature SnBi-Containing solder pastes mixed with lead-free solder balls. Rochester Institute of Technology; 2016.
[17] Luan T, Guo W, Yang S, Ma Z, He J, Yan J. Effect of intermetallic compounds on mechanical properties of copper joints ultrasonic-soldered with Sn-Zn alloy. 2017. https://doi.org/10.1016/j.jmatprotec.2017.04.019.
[18] Abtew M, Selvaduray G. Lead-free solders in microelectronics. Mater Sci Eng R Rep 2000;27:95–141.